CONF-950112--6-Rev.1

GA–A22050
Revision 1

ELECTRON CYCLOTRON HEATING AND CURRENT DRIVE: PRESENT EXPERIMENTS TO ITER

by

R.W. HARVEY, W.M. NEVINS, G.R. SMITH,
B. LLOYD, M.R. O'BRIEN, and C.D. WARRICK

AUGUST 1995

GENERAL ATOMICS

GA–A22050
Revision 1

ELECTRON CYCLOTRON HEATING AND CURRENT DRIVE: PRESENT EXPERIMENTS TO ITER

by

R.W. HARVEY, W.M. NEVINS,[†] G.R. SMITH,[†]
B. LLOYD,[‡] M.R. O'BRIEN,[‡] and C.D. WARRICK[‡]

This is a preprint of a paper presented at the 9th Joint Workshop on Electron Cyclotron Emission and Electron Cyclotron Resonance Heating, January 22–26, 1995, Borrego Springs, California, and to be printed in the *Proceedings.*

Work supported by
U.S. Department of Energy Contracts
DE–AC03–89ER51114 and W–7405–ENG–48,
and by Contract DE-AC03-94SF20282
via Raytheon/Ebasco Subcontract ITER–GA–4002

[†] Lawrence Livermore National Laboratory
[‡] UKAEA/Euratom Fusion Association

GENERAL ATOMICS PROJECTS 3940 and 3994
AUGUST 1995

GENERAL ATOMICS

DISCLAIMER

Portions of this document may be illegible in electronic image products. Images are produced from the best available original document.

Electron Cyclotron Heating and Current Drive: Present Experiments to ITER

R.W. HARVEY, W.M. NEVINS,† G.R. SMITH,† B. LLOYD,‡
M.R. O'BRIEN,‡ and C.D. WARRICK‡
General Atomics
San Diego, California 92186-9784, U.S.A.

Abstract

Electron cyclotron (EC) power has technological and physics advantages for heating and current drive in a tokamak reactor, and advances in source development make it credible for applications in ITER. Strong single pass absorption makes heating to ignition particularly simple. The optimized EC current drive (ECCD) efficiency ($\langle n \rangle IR/P$) shows a linear temperature scaling at temperatures up to $\sim$ 15 keV. For temperatures above 30 keV, the efficiency saturates at approximately $0.3 \cdot 10^{20}$ A/(m^{2}W) for a frequency of 220 GHz in an ITER target plasma with toroidal field of 6 T, due primarily to harmonic overlap [G.R. Smith *et al.*, Phys. Fluids **30** 3633 (1987)] and to a lesser extent due to limitations arising from relativistic effects [N.J. Fisch, Phys. Rev. A **24** 3245 (1981)].

The same efficiency can also be obtained at 170 GHz for the same plasma equilibrium except that the magnetic field is reduced to $(170/220) \times 6$ T $= 4.6$ T. The ECCD efficiencies are obtained with the comprehensive 3D, bounce-averaged Fokker-Planck CQL3D codes [R.W. Harvey and M.G. McCoy, Proc. IAEA TCM/Advances in Simulation and Modeling in Thermonuclear Plasmas 1992, Montreal], and BANDIT3D [M.R. O'Brien, M. Cox, C.D. Warrick, and F.S. Zaitsev, *ibid.*].

† Lawrence Livermore National Laboratory, Livermore, California, U.S.A.
‡ UKAEA Government Division, Fusion, Culham, Abingdon, Oxon OX14 3DB, U.K.

1. Introduction

Electron cyclotron resonant frequency (ECRF) waves provide a source of auxiliary power for heating to ignition that can be injected into the ITER tokamak through a simple launching structure. This paper examines injection of ordinary mode radiation from the outboard side of the tokamak at frequencies near the fundamental cyclotron frequency. This is the preferred approach because of higher density limits. Absorption can be strong and localized near the plasma center, even in high density and temperature operation. In particular, the plasma density has a minor parametric effect on the plasma heating up to densities in the vicinity of the cutoff density, $n_e \approx 3.6 \times 10^{20}$ m^{-3} at 170 GHz. Besides heating, electron cyclotron (EC) waves can fulfill a variety of roles in ITER, for example, startup assist, instability control, and current drive (CD).

In the present paper we report the results of extensive calculations to examine optimizing EC current drive (ECCD) by frequency and injection angle in an ITER, ignited, target plasma. For 220 GHz at 6 T, the ECCD efficiency $\langle\gamma\rangle = \langle n\rangle IR/P$ shows linear temperature scaling up to 15 keV, where $\langle n\rangle$ is line averaged electron density, I is the driven current, R is the major radius of the magnetic axis, and P is the injected rf power. For temperatures above 30 keV, the efficiency saturates at approximately

$$\langle\gamma\rangle = 0.3 \times 10^{20}\ \mathrm{A/W\text{-}m^2} \quad ,$$

assuming a microwave beam launched from the plasma mid-plane at a launch angle $\phi = 40$ deg from the normal to the plasma surface.

The ITER JCT has recommended 170 GHz as the frequency for the ITER ECRF heating and CD system. The above efficiency can also be obtained at 170 GHz for the same plasma equilibrium except that the magnetic field is reduced accordingly to $(170/220) \times 6\ \mathrm{T} = 4.6$ T.

Present high power gyrotrons operate at frequencies up to $\sim$ 160 GHz. At these lower, technologically more advantageous frequencies, the CD efficiency in full toroidal field simulations peaks at angles closer to the perpendicular, and is lower in magnitude. At f = 170 GHz and full field equilibrium, the peak efficiency is $\gamma \approx 0.19\times10^{20}$ A/W-m^2 at a launch angle of approximately 22 deg from perpendicular.

2. Description of CQL3D/BANDIT3D

The results reported here have been obtained with the CQL3D Fokker-Planck and ray-tracing code [1]. The same results, to close approximation, have been independently obtained with BANDIT3D [2] for the 20 and 30 keV cases reported here. The rf power densities are sufficiently low that the distribution function is observed to remain nearly Maxwellian [3]. The Fokker-Planck packages in these codes incorporate the effects of momentum conserving electron-electron collisions which contribute typically $\sim$ 20% to the increased CD efficiency compared to models which omit the current carried by the bulk electrons due to collisions with the tail.

The codes are bounce-averaged, 2–D in momentum space, 1–D in the plasma radial variable, and are fully relativistic. Noncircular plasma geometry and the finite angular width of the injected microwave beam are accounted for using actual ITER free-boundary equilibria. Thus, the detailed effects of geometry on CD efficiency are taken into account. Note, however, that CQL3D assumes an up-down symmetric plasma, whereas this restriction is removed in BANDIT3D. Since ITER is a single-null device, it is necessary with CQL3D to symmetrize the plasma by averaging the upper and lower elongation and triangularity before modeling the ECRF CD and heating. Both codes include a capability of modeling diffusive radial transport of the distribution function, but this effect is assumed negligible for present purposes.

The codes have been benchmarked by comparison between code results and analytical derivations of the neoclassical conductivity [4] (which verifies that the codes correctly handle collisions between passing and trapped particles) and with independent calculations of relativistic fundamental electron cyclotron absorption [5] (which verifies the codes' quasilinear diffusion package and the treatment of the wave polarization). Comparisons with similar 3–D Fokker-Planck codes for a DIII–D experimental situation which was particularly sensitive to several competing effects such as trapping, tail formation, and dc electric field/EC synergy, showed good agreement amongst the codes [6].

The parasitic overlap of the second harmonic absorption with that of the primary first harmonic [7] has been accounted for in the codes. The ECRF wave polarizations from a relativistic dispersion code [5] are used with the relativistic rf quasilinear operator to obtain the ECRF wave damping. Interestingly, the second harmonic generally contributes a small *positive* component to the CD [8]. At 170 GHz the fractional power absorption due to the second harmonic resonance remains less than 30%. At higher frequencies, the second harmonic absorption becomes substantial (reaching nearly 100% at small launch angles). This results in a substantial degradation in the CD efficiency at the lower injection angles. This effect is also a function of aspect ratio, becoming more significant for smaller aspect ratio tokamaks.

3. Heating and Current Drive in 24 MA, 30 keV Discharges

Electron cyclotron heating (ECH) and CD was modeled in a 24 MA reference ITER discharge, using a plasma configuration after Bulmer [9] (modified to be up-down symmetric). The toroidal magnetic field is 6.0 T at $R = 7.7$ m, and the magnetic axis is at $R = 8.43$ m. The plasma has a volume averaged density of $1.54 \times 10^{20}\ \mathrm{m}^{-3}$ with a very flat density profile of the form $n_e = n_{eo}(1-\rho^2)^{0.1}$, and a peaked temperature profile of the form $T_e \sim (1-\rho^2)^2$. (ρ is a normalized minor radius from 0 at the magnetic axis to 1.0 at the separatrix. For CQL3D, ρ is proportional to the square root of the toroidal flux in a flux surface.) A microwave beam with a divergence of 10 deg (full width) was modeled by a bundle of 18 rays. The beam was launched in the plasma midplane at $R = 11.2$ m. The angle between the initial wave vector and the normal to the flux surface ϕ was varied between 5 to 50 deg in the toroidal direction, and the ECRF frequency was varied between 160 and 240 GHz.

The results of our survey of CD in a target plasma with $T_{eo} = 30$ keV are shown in Fig. 1. The CD efficiency depends strongly on both the ECH frequency and on the launch angle ϕ. For each ECH frequency there is an optimal launch angle $\phi_{\max}$ at which the CD figure-of-merit takes on its maximum value $\langle\gamma\rangle_{\max}$.

We see that $\langle\gamma\rangle_{\max}$ increases by a factor of two as the ECRF frequency is increased from 160 to 220 GHz. This increase in efficiency reflects a complex interplay between the increase in the frequency upshift at the location of wave absorption (which results in a corresponding increase in the energy of the resonant electrons, leading to an increase in the CD figure-of-merit), parasitic second-harmonic absorption (which generally increases with increasing ECH frequency and electron temperature, and leads to a reduction in the CD figure-of-merit), and the location of the microwave power absorption (electron trapping effects, which can greatly reduce the ECRF current drive efficiency, increase rapidly as the absorption moves away from the magnetic axis).

These results can be further understood with the help of Fig. 2. As a function of ECRF launch angle ϕ, the figures give the CD figure-of-merit $\langle\gamma\rangle$, the radial location of the peak in the driven current profile $(r/a)_{\max}$, and the fractional absorption due to the second harmonic resonance, for frequency 170 GHz [Fig. 2(a)] and 200 GHz

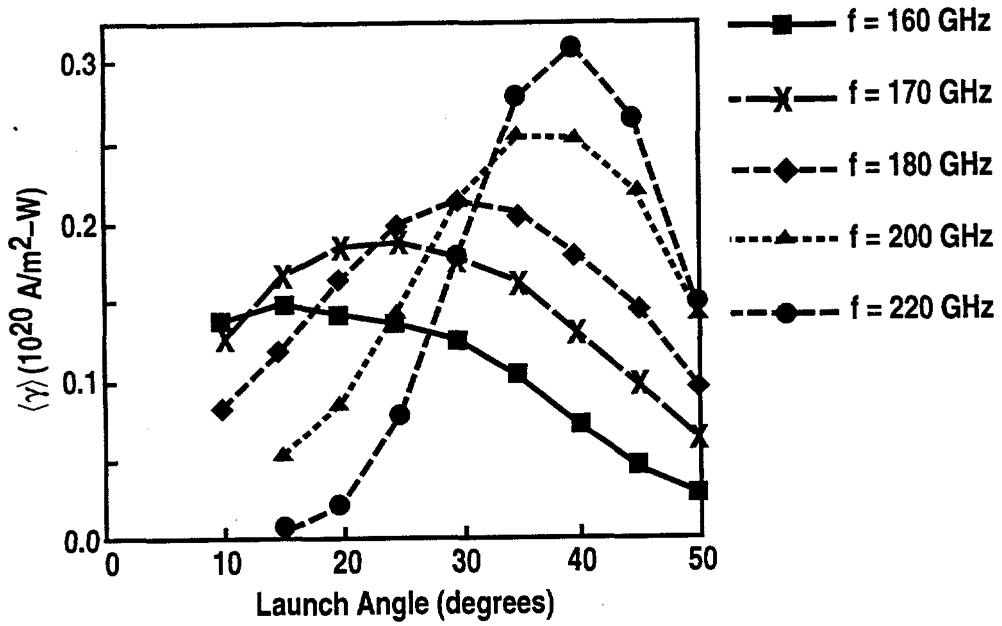

FIG. 1. CD figure-of-merit for a 24 MA target plasma with T_{e0} = 30 keV. The figure-of-merit $\langle\gamma\rangle$ is plotted against launch angle ϕ for a variety of ECRF frequencies.

[Fig. 2(b)]. Also recall that, due to relativistic effects, as EC energy propagates along the rays from the outboard side of the tokamak there is no fundamental harmonic absorption until the point where

$$\left(\frac{\omega_c}{\omega}\right)^2 = 1 - n_{\|pp}^2 \quad , \tag{1}$$

where ω_c is the local cyclotron frequency, ω is the wave frequency, and $n_{\|pp}$ the local refractive index at this "pinch point." In the cases studied here at densities significantly below the cutoff densities, $n_\|$ remains close to its vacuum value and thus $n_\|$ increases toward 1.0 as the launch angle increases. At the pinch point, where the relativistic resonance condition along the ray first becomes satisfied, the energy of resonance particles is $E_{pp} = (\gamma_{pp} - 1)\, mc^2$, where

$$\gamma_{pp}^2 = \frac{1}{1 - n_{\|pp}^2} \quad . \tag{2}$$

The major radius of the pinch point R_{pp} relative to that of the resonance $\omega = \omega_c$-layer R_c is also

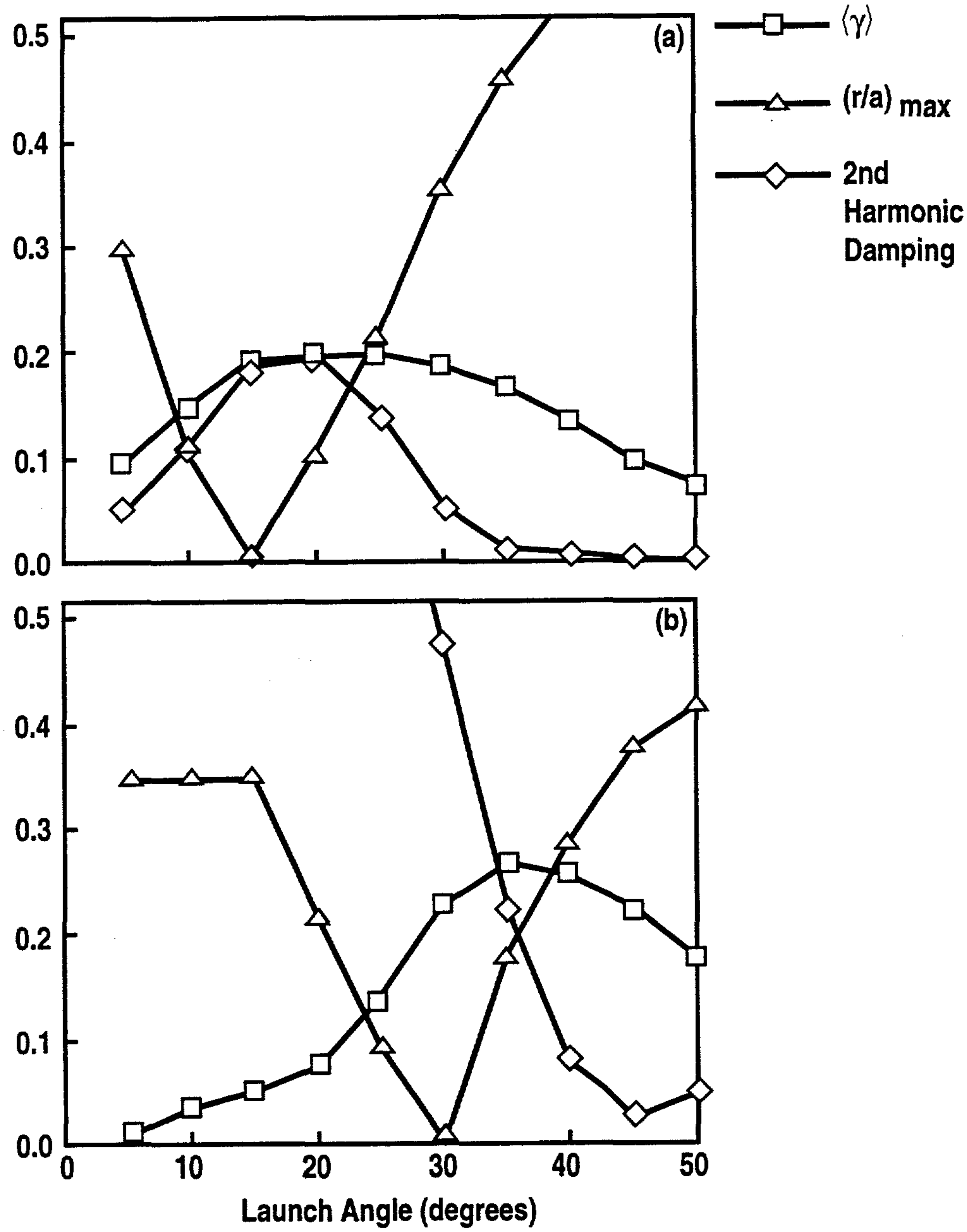

FIG. 2. (a) Current drive figure-of-merit $\langle\gamma\rangle$, radial location of the peak of the driven current profile $(r/a)_{\max}$, and the fractional absorption due to the second harmonic resonance are plotted against launch angle ϕ. This is for 170 GHz radiation launched into the same 24 MA target plasmas at 30 keV as used in producing the data in Fig. 1. (b) Results at 200 GHz; otherwise the same as (a).

$$\left(\frac{R_{pp}}{R_c}\right)^2 = \frac{1}{1-n^2_{\|pp}} \quad , \tag{3}$$

where the magnetic field variation in ω_c has been approximated as R^{-1}. Thus as the launch angle is increased, $n_{\|pp}$, γ_{pp}, and the resonant energy all increase. But also the major radius R_{pp} of the pinch point increases. When R_{pp} becomes greater than the major radius at the magnetic axis R_{mag}, the efficiency is degraded due to trapping. Also, the peaking of the temperature profile at the magnetic axis favors maximization of $\langle\gamma\rangle$ near the magnetic axis. Thus as the frequency increases, R_c becomes smaller, and $n_\|$ can be increased to give greater energy E_{pp} and efficiency, still keeping R_{pp} near R_{mag}.

The parasitic loss of EC power due to the second harmonic overlap [7] is the major factor which prevents attainment of even greater efficiency by going to higher and higher frequency (and launch angle). At 170 GHz and $T_{eo} = 30$ keV, [Fig. 2(a)], the second harmonic damping is 20% at the launch angle (20 deg) of maximum CD efficiency. At 200 GHz [Fig. 2(b)], the second harmonic damping is pushing the optimum CD angle to greater than 35 deg. At 240 GHz, the parasitic second harmonic absorption dominates at all injection angles. This parasitic loss of EC power due to second harmonic overlap is a dominant factor.

An additional consideration is that at a launch angle of 45 deg, the rays just graze the magnetic axis. At higher angles, the rays only pass outside of the magnetic axis, where trapping effects reduce the CD efficiency. This pulls down the CD efficiency at angles greater than 45 deg.

4. Current Drive at Reduced Magnetic Field

We expect the current drive efficiency to vary with ECRF frequency mainly as a function of the ratio between the wave frequency and the electron cyclotron frequency at the magnetic axis. Hence, if the B-field of the target plasma is reduced by the amount $(170/220) \approx 0.77$, the electron cyclotron CD efficiency at 170 GHz should be nearly equal to that obtained at 220 GHz in a full-field target plasma. We investigate this by comparing the CD figure-of-merit computed for 220 GHz waves injected into a 6 T target plasma with a central temperature, $T_{eo} = 30$ keV, with that obtained when injecting 170 GHz waves into a target plasma in which B_0 is reduced to $(170/220) \times 6$ T $= 4.636$ T. The results of this survey are shown in Fig. 3 below.

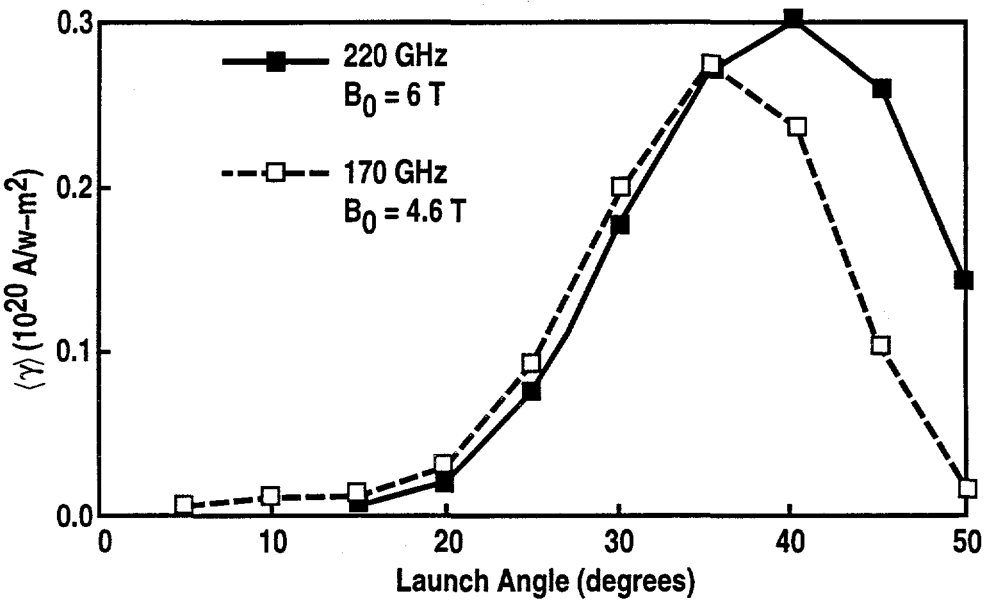

FIG. 3. The CD figure-of-merit $\langle\gamma\rangle$ for 220 GHz ECRF waves injected into a 6 T target plasma (solid line) and for 170 GHz waves injected into a 4.636 T target plasma (dashed line). In both target plasmas, the temperature and density were held fixed at $T_{e0} = 30$ keV and $n_{e0} = 1.7 \times 10^{20}$ m^{-3}.

We see that the reduction in the peak CD figure-of-merit is less than 10%, with $\langle\gamma\rangle$ peaking at 0.28×10^{20} A/W-m^2 for 170 GHz into the $B_0 = 4.636$ T target plasma, versus $\langle\gamma\rangle = 0.30 \times 10^{20}$ A/W-m^2 for 220 GHz into the $B_0 = 6$ T target plasma. The slight reduction in efficiency seems to be related to a reduction in opacity which occurs for the lower frequency/B-field combination. Thus the technically accessible source frequency 170 GHz can give the highest efficiencies by reducing the B-field.

5. Optimized Current Drive Efficiency Versus T_{eo}

Sets of runs have been performed at various temperatures, varying launch angles, and wave frequency, as in the previous 30 keV case. At each temperature, results are obtained similar to those shown in Fig. 1.

The peak (*i.e.*, optimized) efficiencies obtained in each of these runs are presented in Fig. 4 as a function of T_{eo}. Results are given for the ± 5 deg divergence (10 deg FW) 18-ray cases such as in Fig. 1, as well as for single ray cases with the narrow T_e-profile $\sim (1-\rho^2)^2$, and with a broader temperature profile, $T_{eo} \sim (1-\rho^2)$. Also shown are experimental points which we will briefly discuss below.

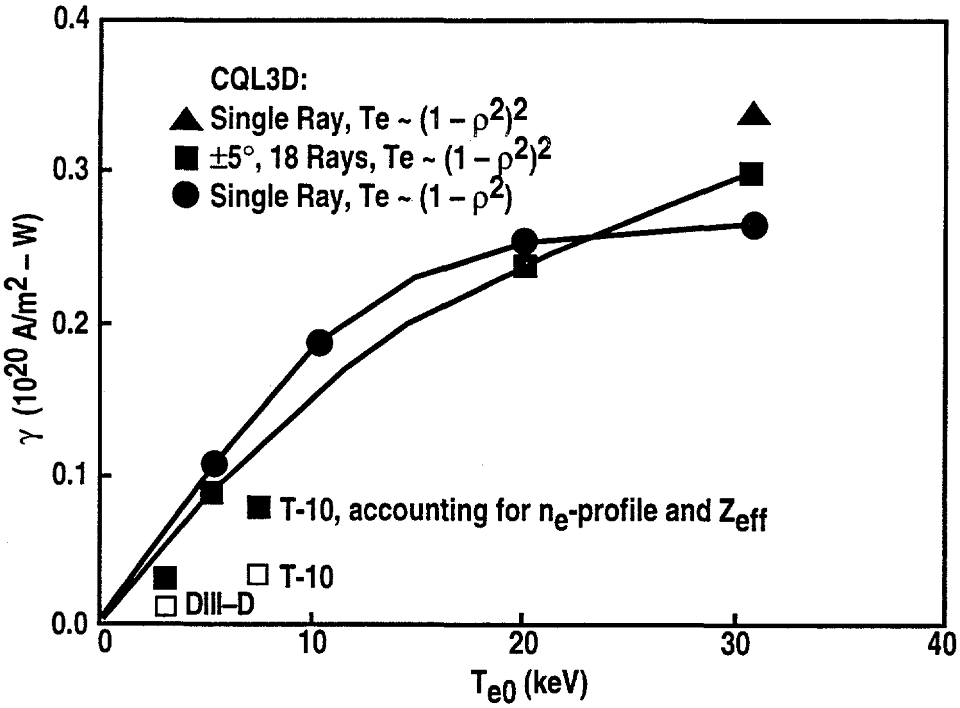

FIG. 4. Optimized CD efficiency versus central plasma temperature for the 24 MA target plasmas. Curves are shown for single ray models for two different temperature profiles, and for a model with 10 deg divergence in the launch angle. Experimental results are shown for comparison.

The main feature is that the CD efficiency exhibits a saturation setting in above central electron temperature ~ 20 keV. The major cause of the saturation is the second harmonic overlap. As the temperature increases, the resonant energy E_{pp} of the pinch point can be increased in accord with Eq. (2) still obtaining sufficient damping. The increasing resonant energy leads to greater CD efficiency, in accord with the Fisch-Boozer mechanism [10]. But the wave frequency must also be increased in accord with Eq. (3), to keep the pinch point near the plasma center. As the wave frequency is increased, the second harmonic overlap becomes more of a limiting factor. At $T_{eo} = 20$ keV, the second harmonic absorption is a significant factor in degrading CD efficiency, as evidenced by the difference between the single ray results in the peaked T_e-profile $[\sim (1-\rho^2)^2]$, compared to the broader T_e-profile $\sim (1-\rho^2)$. At 30 keV, second harmonic absorption is moving the peak of the CD efficiency off-axis [see Fig. 2(b)] into the region of trapping-reduction of the efficiency, giving the saturation of efficiency.

A secondary cause for saturation is relativistic effects [11]. For perpendicular diffusion, the CD efficiency is a function of parallel resonance momentum-per-mass $u_{\parallel}$. The efficiency increases proportional to $u_{\parallel}^2$ at low velocity, but maximizes at $u_{\parallel}/c \approx 2$. [for $T_{eo} \lesssim 75$ keV, see Fig. 2(b) of Ref. 11]. At $T_e = 25$ keV, the efficiency at $u_{\parallel}/c = 1$ has achieved about 80% of its $u_{\parallel}/c = 2$-maximum (when there is a parallel component to the QL diffusion [12] then this limit may be relaxed). The maximum CD efficiency which we have obtained at 30 keV is near the absolute maximum consistent with relativistic limits for perpendicular diffusion (usually the case for EC).

Experimental points have been included in Fig. 4 for comparison with the optimized value. The DIII–D results [13] and T–10 results [14] are for fixed launch angles and thus are not optimized over launch angle for the particular experimental conditions obtained, as can be easily done with the codes, but the results have been adjusted upward (from the experimental values represented by the open squares) to account for the quite flat density profile and low $Z_{\rm eff}$ assumed in these studies. Evidently the experimental efficiency improves with T_e but much higher temperature plasmas are required to achieve the full CD efficiencies that EC waves are capable of. Future work will focus on optimization of off-axis CD for profile control in advanced tokamak operations.

6. Conclusions

The CQL3D and BANDIT3D Fokker-Planck codes have been used to calculate the maximum current drive efficiencies γ obtainable in ITER/EDA for EC waves launched at the outer equatorial plane of the tokamak. At low temperature, the optimized efficiency scaled approximately linearly with plasma temperature T_{eo}. At 20 keV, onset of a saturation of γ was evident, and at 30 keV, the maximum efficiency is $0.3 \cdot 10^{20}$ A/(m^2·W). The optimal wave frequency in a full field ITER equilibrium at 30 keV is approximately 220 GHz at launch angle 40 deg from perpendicular in the toroidal direction. Approximately the same efficiency can be obtained at 170 GHz, if the plasma magnetic field is proportionately reduced.

7. Acknowledgments

R.W.H. wishes to acknowledge contributions by Drs. Y.R. Lin-Liu and S.C. Chiu in verification of CQL3D.

This is a report of work supported by U.S. Department of Energy Contracts DE-AC03-89ER51114 and W-7405-ENG-48, and by Contract No. DE-AC03-94SF20282 via Raytheon/Ebasco Subcontract ITER-GA-4002. Part of the work was jointly funded by the U.K. Department of Trade and Industry and Euratom.

8. References

[1] R.W. Harvey and M.G. McCoy, in *Proc. IAEA TCM on Simulation and Modeling of Thermonuclear Plasma, Montreal, 1992* IAEA, Vienna, 1993) p. 489.

[2] M.R. O'Brien, M. Cox, C.D. Warrick, and F.S. Zaitsev, *ibid.*, p. 527.

[3] R.W. Harvey, M.G. McCoy, and G.D. Kerbel, Phys. Rev. Lett. **62** (1989) 462.

[4] J.W. Connor, R.C. Grimm, R.J. Hastie, and P.M. Keeping, Nucl. Fusion **13** (1973) 211.

[5] E. Mazzucato, I. Fidone, and G. Granata, Phys. Fluids **30** (1987) 3745.

[6] E. Westerhof, this conference.

[7] G.R. Smith, R.H. Cohen, and T.K. Mau, Phys. Fluids **30** (1987) 3633.

[8] B. Lloyd, M.R. O'Brien, and C.D. Warrick, in *Proc. 211st Euro. Conf. on Contr. Fusion and Plasma Heating, Montpellier, 1994* Vol. II, p. 1012.

[9] R.H. Bulmer, Lawrence Livermore National Laboratory, equilibrium 93046-2, personal communication (1993).

[10] N.J. Fisch and A.H. Boozer, Phys. Rev. Lett. **45** (1980) 1549.

[11] N.J. Fisch, Phys. Rev. A **26** (1981) 3245; C.F.F. Karney and N.J. Fisch, Phys. Fluids **28** (1985) 116.

[12] R.H. Cohen, Phys. Fluids **30** (1987) 2442; A.Yu. Kuyanon *et al.*, Kurchatov Institute-Russian Research Center Rept. IAE-5790/6 (1994).

[13] R.A. James *et al.*, Phys. Rev. A **45** (1992) 8723.

[14] V.V. Alikaev *et al.*, Nucl. Fusion **32** (1992) 1811.